From Lung Images to Lung Models: A Review

S. L. A. Lee, A. Z. Kouzani, and E. J. Hu

Abstract—**Automated 3D lung modeling involves analyzing 2D lung images and reconstructing a realistic 3D model of the lung. This paper presents a review of the existing works on automatic formation of 3D lung models from 2D lung images. A common framework for 3D lung modeling is proposed. It consists of eight components: image acquisition, image pre-processing, image segmentation, boundary creation, image recognition, image registration, 3D surface reconstruction, and 3D rendering and visualization. The algorithms used by the existing systems to implement these components are also reviewed.**

I. INTRODUCTION

HUMAN lung contains an airway tree that consists of 19 generation of dichotomous branching in the airways travelling from the trachea to the alveolar sacs [1]. A number of diseases affect the lung and impair its functions. Currently lung diseases are diagnosed in several ways including lung imaging techniques.

3D lung modeling refers to the process in which automated algorithms process 2D medical lung images of a person, and then form a realistic 3D model of the person's lung (see Fig. 1). The main application of the 3D lung modeling is to enhance the accuracy of the lung disease detection practice through lung imaging methods.

The 3D lung modeling is a challenging task due to the fact that the existing lung imaging methods are incapable of visualizing the entire 19 generation of the lung airway tree [2]. The resolution of each image and the spatial distance between two consecutive image frames are vital factors dictating the accuracy and reliability of the reconstructed 3D lung model. In addition, the computational complexity is also an important factor.

This paper presents a review of the research into automatic creation of 3D lung models from 2D lung images. It proposes a common framework for the 3D lung model reconstruction, and provides a description of the specific algorithms used by each existing system to implement each of the eight components.

II. LUNG IMAGING METHODS

Lung imaging methods are mainly used to visualize and detect various lung diseases. There exist two major lung imaging methods [3, 4]: computed tomography (CT) and magnetic resonance imaging (MRI). They provide 2D lung image datasets for direct inspection, or for reconstruction of 3D lung models.

The first electro-magnetic-interference CT scanner was launched in 1972. Computed axial tomography (CT scan or CAT) is a medical imaging technique which is based on X-ray imaging. The latest model of CT scanners can produce up to 3 rotations per second with a resolution of up to 0.33 mm^3 voxels with the z-axis scan speed of up to 18 cm/s. CT images are used to identify a particular disorder as the scan provides 0.33 mm thinness between the two neighboring slices.

The MRI scanners were introduced around 1980. MRI is based on radio waves hitting the protons in water molecules. A magnetic field changes the protons' position, producing signals that form 2D images. These images show differences in water content between various tissues.

MRI is not as good as CT in showing lung defects because it requires more time to obtain a scan [1]. The images may get distorted due to the movement of the heart and lungs during the scan. Although MRI provides resolution with better contrast compared to CT, it produces less image slices than that of CT. Therefore, CT is preferable for radiologist and researchers in modeling the 3D lungs, while MRI can be more suitable to be used to clarify findings from those CT scans.

III. EXISTING LUNG MODELING TECHNIQUES

Considering the existing literature on 3D lung modeling from 2D lung images, we have devised a common framework to represent the important stages involved in the reconstruction of 3D lung models. Fig. 2 illustrates this common framework. It consists of eight components: image acquisition, image pre-processing, image segmentation, boundary creation, image recognition, image registration, 3D surface reconstruction, and 3D rendering and visualization.

Fig. 1. A 3D model of a person's lung [5] .

2377

Different existing approaches employ only a different subset of these components. For example, Burton et al. [6], Betke et al. [7], and Bartz et al. [8] do not use the boundary creation and the recognition components. On the other hand, Nakada et al.[9], Zhang et al. [10], Antonelli et al. [11] employ only one of the boundary creation or the recognition components. And Zhou et al.[12] however utilizes both the boundary creation and the recognition components.
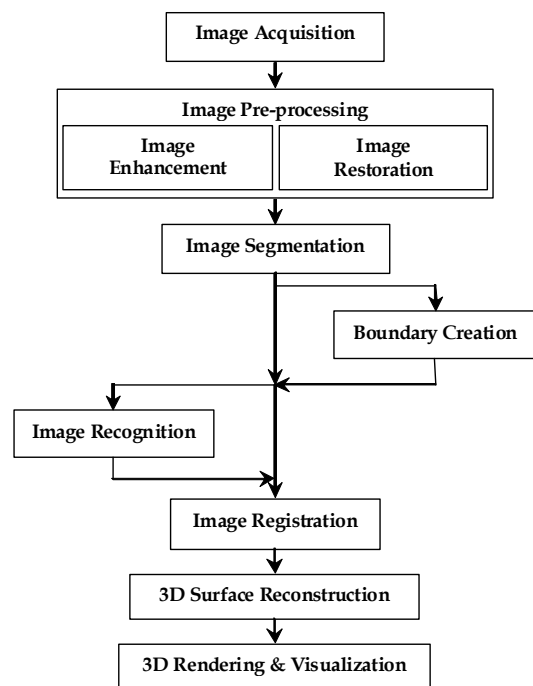
```
┌─────────────────────────────┐
│      Image Acquisition      │
└─────────────────────────────┘
┌─────────────────────────────┐
│    Image Pre-processing     │
│ ┌──────────┐ ┌────────────┐ │
│ │  Image   │ │   Image    │ │
│ │Enhancement│ │ Restoration│ │
│ └──────────┘ └────────────┘ │
└─────────────────────────────┘
┌─────────────────────────────┐
│     Image Segmentation      │
└─────────────────────────────┘
          ┌──────────────────┐
          │ Boundary Creation│
          └──────────────────┘
┌──────────────────┐
│ Image Recognition│
└──────────────────┘
┌─────────────────────────────┐
│     Image Registration      │
└─────────────────────────────┘
┌─────────────────────────────┐
│   3D Surface Reconstruction │
└─────────────────────────────┘
┌─────────────────────────────┐
│  3D Rendering & Visualization│
└─────────────────────────────┘
```

Fig. 2. Our devised common framework for 3D lung model reconstruction.

A. Image Acquisition

Image acquisition is the process of acquiring 2D CT or MRI lung image datasets. Most existing works used lung datasets from collaborative hospital partners of patients whose data was made anonymous. However, Garrity et al. [5] used the visible-human CT image datasets from National Library of Medicine [13]. Lung imaging researchers initially started with using CT or MRI datasets, and then expanded their scopes on CT datasets with virtual bronchoscopy (Bartz et al. [8] and Fetita et al. [14]), MRI datasets with SPECT (Burton et al. [6]), and SPECT datasets (Martenon et al. [15]). Virtual bronchoscopy is a computer generated model using multi-detector helical CT which is a recent technical development that allows visualization of the lumen and wall of the trachea and proximal part of the bronchial tree [16].

There exist four popular public lung image databases namely: (i) Early Lung Cancer Action Program (ELCAP) Public Lung Image Database [17] by Cornell University, (ii) ELCAP Public Lung Database to Address Drug Response [18] by Cornell University, (iii) National Imaging Archive [19] by National Cancer Institute, and (iv) Medical Image Database [20] by Smirniotopoulos.

B. Image Pre-processing

Image pre-processing is the process of improving both the accuracy and interpretability of the acquired lung images. Based on our review of the existing literature, not all 3D lung modeling papers describe the image pre-processing component. There are existing works on background removal in pre-processing stage which use an image operator to move around four direction of the four corners (Antonelli et al. [11] and Tan et al. [21]). Zhang et al. [10] applied ridgeness operator to enhance the contrast of the original CT image datasets.

The image pre-processing component can be further divided into two groups:

1) *Image Enhancement:* Image enhancement is the process of improving the detectability of the CT or MRI lung image datasets. Band pass filtering method is employed by Lo et al. [22] to extract the structure whose size was less than 3cm to extract the alveoli. Also, intensity-based matched filtering was utilized to identify the vessels, airway, nodules and other circular spots. Histogram equalization was used in Tan et al. [21] to enhance the contrast of the lung images.

2) *Image Restoration:* Image restoration is the process of reducing various degradations of lung images to an ideal state. According to Kitasaka et al.[23], Laplacian of Gaussian filters act as the sharpening operator to enhance the bronchial wall. Some researchers used Gaussian filter by means of a sync function (e.g., Nakada et al. [9]), and some used fixed standard deviation (e.g., Tozaki et al. [24]) to smooth the images. Yim et al. [25] extracted the airway initially by means of median filtering to prevent threshold outburst in the lung parenchyma. Later, Tan et al. [21] used a 2×2 and 3×3 median filters for mask and base images respectively to reduce the presence of speckle noise. Low frequency filter was chosen over high frequency filter to avoid bronchial wall discontinuity in Fetita et al. [14]. Several rounds of majority filtering were utilized by Warren et al. [26] to smoothen the lung images respectively, and eliminate the interior high-density voxels.

C. Image Segmentation

Image segmentation is the process of classifying the objects of interest in the lung images into constituent regions. The existing work on segmentation can be classified into thresholding, watershed transformation, region growing, component labeling, anatomical landmark segmentation, and so on.

In Hu et al. [27], optimal thresholding was used to separate the low density lung area from the higher density surrounding tissue. Topological analysis was used for filling expelled lung regions during the thresholding process which eradicated the inner cavities. Binary morphological erosion was applied to recover the un-joined left and right boundary. Ukil and Reinhardt [28] used a fast 3D morphological

closing with ellipsoidal kernel which smoothed the lung boundary. Thresholding for the first nine generation of the airway cast were employed due to the high contrast between the plastic and the air by Sauret et al. [29]. They stated that thresholding was practical for the trachea, primary and secondary airway as the thick airway walls provided high contrast with the background. On the other hand, the smaller airways had thin walls and thus the contrast between the air and the tissue were relatively low which made it undesirable. Schmidt et al. [30] implemented a threshold based algorithm, in which initially the seed-point was determined by the user to gather the entire high-intensity voxels above the predefined threshold. The thinning algorithm was performed to derive the skeletonized airway structure followed by erosion to ensure the removal of the particular voxels maintaining the airway model. Antonelli et al.[11] applied dynamic threshold and binary morphological operators to improve the boundary and fill up the hole. Areas with high contrast were detected by Sobel operator and thinning algorithm was utilized to reduce the border to one pixel width. Canny edge detector with low and high thresholds was used by Tan et al. [21] to extract the edges. Thresholding of the CT datasets into binary images were discussed in Warren et al. [26] model.

3D watershed transformation was employed by Kuhnigk et al. [31] to detect the lobar fissures with low variability using different manual intervention. This method was proven sensitive to the vessel tree segmentation. Shojaii et al. [32] presented a 2D marker based watershed transformation where the right and left lungs were separated automatically by the thin edge technique in the watershed transformation. Therefore, watershed transform eradicated the optimal thresholding task, and then the separation of the left and right lungs saved the computational time (Hu et al. [27], Zhang et al. [10], and Antonelli et al. [11]). Another advantage of marker based watershed transform over standard watershed transform applied to the gradient image was to avoid over-segmentation where marker based decreased the regional minimum and connect them with the region of interest.

Fig. 3 shows sample processed 2D lung images including a segmented 2D lung image.

A simple region growing followed by morphological closing and opening procedure was used to extract the bronchus region by Nakada et al.[9]. An optimal threshold for each branch was defined to avoid miss-segmentation of branches through region growing process. Zhou et al. [12] extracted the airway tree via branch-by-branch basis from the air region by a 3D region growing technique to overcome discontinued branches in the medical images due to leak region. The grey level threshold was determined by discriminant analysis in order to choose the grey level value of the two density distribution based on the histogram. Later, 3D connectivity analysis was used to represent the real chest region by connecting the 18 nearest elements with the largest volume from the tissue region and eliminate the remaining regions. In Yim et al. [25], the step to exclude the high density vessel and to fill the region and eliminate the interior cavities were eradicated by applying an inverse seeded region growing for lung extraction algorithm. For airway extraction, an automatic seed point was selected, and the airway was extracted by applying 3D region growing, 2D binary closing, and dilation operations to remove unwanted cavities.

Binarization and labeling process was performed by Haneishi et al. [33] to extract the right and left lung, and bronchi of the lung images using connected region.

Zrimec and Busayarat [34] characterized the lung region based on the anatomical landmarks such as sternum, vertebrae with the spinal canal, trachea, carina and hilum. Trachea, sternum, and vertebrae were segmented using fixed threshold morphological operators. This is done to ensure a smooth and noise free boundaries, and also a connected component labeling based on the knowledge provided in the anatomy frame. Carina was distinguished based on the information where trachea begins to diverge and hilum recognition was based on the curvature analysis. Main bronchi were removed before segmentation to detect the lung parenchyma. The entire lung was segmented using snake contour and morphological operators. Misra et al. [35] performed the same segmentation technique as Zrimec and Busayarat [34] which referred to the anatomical landmarks to segment the lung.

Garrity et al.[5] manually segmented the contour using the SURFdriver package. Bartz et al. [8] segmented the blood vessel, trachea, and bronchial using SegoMeTex tool. 3D region growing method was used to extract the airway based on the starting seed point at the trachea. Masking technique was utilized to eliminate leakages in the smaller airway. Later, 2D wave propagation was used to complete the high and middle branches followed by 2D template matching to segment small lumen which is approximately one voxel size. If there were no significant changes in the previous stage, the iterative loop ended.

Mean shift based image segmentation algorithm was applied by Okada et al. [36] which integrate spatial probabilistic function to segment challenging wall-attached nodule in CT lung images. It requires some manual intervention from human expert. Lately Sun et al. [37] performed region-growing and mean shift algorithm to find the nodule boundary. As mean shift approach is susceptible to the changes in the granularity and color bandwidth features, a comprehensive rule to obtain the suitable bandwidth is discussed in [37].

Xu et. al.[38] proposed a graph cuts based active contours algorithm to overcome the conventional graph-based favoring short-boundaries cut resulting in small regions. It is proven that this segmentation algorithm is able to segment small lung nodule as well as edge discontinuities on boundary. Normalized cuts segmentation algorithm is another method to avoid graph-based biasing by introducing a cost function called disassociation. Chen et. al. [39] employed normalized cuts to identify the atypical properties of severe acute respiratory syndrome (SARS) in lung scan. The normalized cuts algorithm provided an unsatisfactory

result because the lung fields in the SARS images is not adequately visible.

D. Boundary Creation

Boundary creation is the process of delineating the boundary and airway of the segmented lung image datasets. In the image segmentation, the segmented image contains only a set of pixel points belonging to a target region but does not provide boundary information especially the sequence of the pixel point of the boundary [40-42]. This task is carried out by the boundary creation process.

There are only a few published works that used a boundary creation component in their system structures. For example, Antonelli et al. [11] calculated the Euclidean distance between the border points and compared it with a predefined threshold. Another vital condition before establishing the line between two points was validating that the two points were not the internal points of the lung. Zhou et al. [12] performed a 2D border following procedure to trace the outline of the border of the human lung between the air region and the tissue region. Warren et al. [26] employed a semi-automated border creation method using a shortest path technique by the Dijkstra's algorithm.

E. Image Recognition

Image recognition refers to the process of analyzing the image to determine whether a certain object is present in the image or not, and also to identify the location of the object. Recently, some researchers have expanded their focuses into image recognition to improve disease detection. In Kubo et al. [43], Vander Berg linear feature detector was used to extract the fissure of the lobes with morphological operators such as directional disc structure. Liu et al. [44] obtained the extracted texture using 2D Fast Fourier Transform (FFT) and Kohonen self-organizing map (SOM) to classify the FFT extracted features. The advantage of using the FFT over concurrence matrix was that computational cost was reduced. The disadvantage of this system was that manual intervention was required to mark the region. Kitasaka et al. [23] employed Hessian 3×3 matrix to determine the local shape classification and pulmonary pleura. According to Zhou et al. [12], Hessian matrix analysis proved beneficial for vessel extraction but the trade-off was that it required more computational times. Zhang et al. [10] utilized fuzzy logic theory to detect the initial fissure and final fissure of the lung lobes. The initial fissures were initialized by the atlas from CT training datasets and the intersection between the datasets and the atlas were then determined. For final fissure detection, intensity and shape information initialized the 2D fissures from the neighboring point. Zhou et al. [12] analyzed the combination of airway tree lobar and vessels based on the Voronoi division to identify the likelihood of the lobar fissure situated in the lobe. A multilayer-preceptron artificial-neural-network was exploited to indicate five different classes of emphysema based on the severity condition in Tan et al. [21]. The texture was analyzed based on the grey level dependence, run length, and histogram method, accordingly.

F. Image Registration

Image registration is the process of geometrically transforming feature points from two viewpoints representing a scene within two 2D images in order to enable the feature points achieving the same coordinates after transformation. Haneishi et al. [33] performed a rough registration followed by a fine registration to match the centered of the images respectively. Later, iterative Powel multidirectional techniques with Brent 1D match technique were used. Initial landmark registration was used by Betke et al. [7], and it increased the speed significantly. Later, a global registration method was employed to model the region which was sensitive to the changes in the transformation parameters. These changes influenced the corresponding transformation in the medical image datasets. Li et al. [45] utilized intensity-based consistent technique to register each of the template image volume, normalized these transformations, and built a deformable atlas with the normalized transformation. Iterative closest point method of the contours with least square correlation was applied by Lo et al. [22] to determine the global starting point. The ortho-normal transformation matrix was then applied to re-slice the subsequent CT image accordingly to the geometrical position of the first CT image in 3D domain. Fixed reference points such as stable anatomical marker were used with 3D transformation such as scaling, translating and rotating as described by Zrimec and Busayarat [46]. Ray tracing was introduced to locate matching points of two surfaces. The advantage of this technique was that all the registered points were located inside the model. Zhang et al. [10] performed global transformation which scaled the target and source lung to the equal dimension, and translated the position accordingly. Later, local deformation was employed to calculate the best match displacement in order to equate the lung boundary of similar process. Zhou et al. [12] used the 3D Euclidean transformation method by initializing each lobar vessel to the associate lobar region and measure the distance between them.

G. 3D Surface Reconstruction

3D surface reconstruction is the process of establishing a three dimensional surface model which precisely describe the registered image datasets. Garrity et al. [5] used the Rhinoceros non-uniform rational B-spline approach to generate a smooth 3D cubic for each lobe and branch with the corresponding airway tree. This model was an integration of a realistic boundary-airway and an artificial airway. At each terminal branches of the segmented airway, cylinder caps were placed in order to identify the lung lobe surface and store them in a queue. These procedures began from the first branch at the top queue until the entire lung lobe was filled based on the condition of the algorithm to produce the entire airway. A controlled expansion based on energy minimization derived from Markov Random Field algorithm

was used to create the bronchi tree starting from the lower airway generation in Fetita et al. [14]. Bartz et al. [8] utilized the marching cube algorithm to reconstruct the lung surface. Zrimec and Busayarat [46] employed triangle strips to connect the two consecutive slices where the scan-line triangle filling method filled up the strips. Zhang et al. [47] represented the 3D boundary using triangle meshes by FastRBF package. Nakada et al. [9] employed surface fitting algorithm to construct the 3D boundary and airway model. Voronoi diagram and Delaunay tessellation concepts were used in Martonen et al. [15] boundary model to obtain the mathematical mosaic representation allowing integration with 3D asymmetrical airway model.
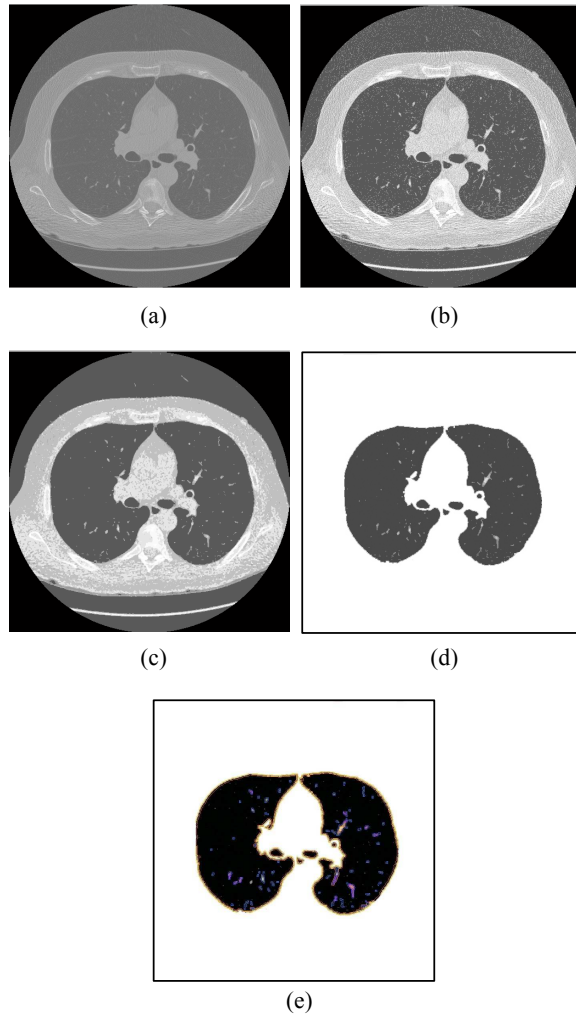

Fig. 3. Sample processed 2D lung images: (a) original from ELCAP [17], (b) enhanced image, (c) restored, (d) threshold, and (e) segmented images.

H. 3D Rendering and Visualization

3D rendering-and-visualization is the process of accurately displaying 2D projections of a 3D hybrid boundary and airway reconstructed model. Once the 3D lung model is created, available computer graphics tools can be employed for rendering and visualization. Garrity et al. [5] utilized a modeling tool to achieve 3D rendering and visualization of the lung surfaces. Zrimec and Busayarat [34] model was visualized using Java-OpenGL tools. IBM Visualization Data Explorer was used by Burton et al. [6] to visualize and render the 3D boundary model. The program produced coarse realistic model due to the fact that no smoothing of surface was performed. Schmidt et al. [30] utilized ILAB4 to perform visualization of their 3D lung models.

IV. DISCUSSIONS

Applications such as lung disease detection inspire researchers to tackle realistic 3D lung reconstruction. We have formulated a common architecture for the 3D lung modeling. Each component in this architecture is summarized to provide an insight into the method used in each existing work.

Considering the image acquisition component, most researchers employed lung datasets from their collaborative hospital partners. Popular public lung CT image databases are available in the public domains such as ELCAP, National Imaging Archive, and Medical Image Database. Looking at the image pre-processing component, it is divided into two sub-categories namely image restoration and image enhancement. Ridgeness operator, majority filter, Laplacian of Gaussian, low frequency filter, background removal, Median filter, Gaussian filter, band-pass filter, and histogram equalization are amongst the techniques utilized in the existing works. Considering the image segmentation component, it is the area on which most researchers have focused. In optimal thresholding, the lung boundary still remains unsmooth. As a remedy, the 3D morphological closing with ellipsoidal kernel is used to overcome the issue. Watershed transformation with a 2D marker segments the right and the left lungs automatically, and saves some computational times. Also over-segmentation issue is dealt with due to the use of marker that decreases the regional minimum, and connects them with the region of interest. Other techniques such as anatomical landmark segmentation, active snake contour, and wave propagation appear not performing satisfactorily. Lately more robust techniques such as mean shift, combination of mean shift and region growing, graph cuts, and normalized cuts are used. Concerning the boundary creation component, not all existing works describe its utilization thoroughly. Only three published papers describe the technique employed for boundary creation namely 2D border following, Euclidean distance-based, and Dijkstra method to find the shortest path. With regard to the image recognition component, it has been recently used to detect lobar fissures using fuzzy logic, Voronoi division, Hessian matrix, FFT/Kohonen SOM, and

neural networks. Hessian matrix is proven to be beneficial for vessel extraction but is computationally expensive. FFT decreases the computational cost significantly.

Considering the image registration component, some works did not develop dedicated algorithms and only used available software tools. Considering the image registration component, ray tracing, global registration, and ortho-normal transformation matrix algorithms were used. An initial landmark registration followed by a global registration has proven to increase registration speed significantly. With regard to the surface reconstruction component, the algorithms used include surface fitting algorithm, mesh, triangle filling, marching cube algorithm, Voronoi diagram and Delaunay tessellation. With regard to the final stage, 3D rendering and visualization component, most existing works rely on the existing 3D rendering and visualization tools usually available in computer graphics.

Most existing works used CT rather than MRI datasets because CT provides more image slices per lung. Majority of the early works focused on the creation of 3D artificial lung airway only. Most reported works dealt with the 3D boundary reconstruction. However, some recent attempts tend to tackle the 3D airway reconstruction as well as the 3D hybrid boundary-airway reconstruction. About the computational complexity, the 3D boundary reconstruction methods tend to be simpler. The 3D airway reconstruction methods are more computationally expensive. However, the 3D hybrid boundary-airway reconstruction approaches possess the highest computational complexity.

This paper has formulated a common framework for 3D lung modeling including eight components. While a comparison of the existing algorithms for each of the components has been described, it was impractical to give a more detailed insight into these areas. Each area is considered a major research field by itself consisting of many research publications. Presentation of a comprehensive study of these publications was not feasible within the limited space of this paper.

The 3D lung modeling research is still concerned with the reconstruction of hybrid artificial-realistic 3D boundary-airway models because the resolution of the 2D lung images is still unsatisfactory. But due to the advancements in the lung imaging technology, we are not far from having access to equipment that would make available higher quality lung images. This will facilitate the development of fully realistic 3D lung boundary-airway models for medical applications.

V. CONCLUSION

This paper gives a study on automatic reconstruction of 3D lung models from 2D lung medical images. A common architecture for the 3D lung modeling is proposed which consists of 8 components. For each reviewed system, the components that were employed are stated. A description of the specific algorithms implementing each component in the reviewed works is also given. While the 3D lung modeling research is still concerned with the reconstruction of hybrid

artificial-realistic 3D models, the rapid advancements in the lung imaging technology are expected to result in the development of fully realistic complete 3D lung models.

REFERENCES

[1] D. Karthikeyan, *High-Resolution Computed Tomography of the Lungs - A Pattern Approach*, 1st ed. London: Hodder Arnold, 2005.

[2] I. C. Sluimer, "Automated Image Analysis of Pathology Lung in CT," in *Image Sciences Institute*, vol. Masters Degree. Utrecht: University Medical Centre Utrecht, Sept. 2005.

[3] "NDT Resource Learning, (homepage of the collaboration with National Science Foundation ATE program in America)," Non-destructive Testing Resource Center (NDT), 2007.

[4] I. R. Radiological Society of North America, "Radiology Info: MRI," 2007.

[5] J. M. Garrity, W. P. Segars, S. Knisley, and B. M. W. Tsui, "Development of a dynamic model for the lung lobes and airway tree in the NCAT phantom," in *IEEE Nuclear Science Symposium Conference Record*, vol. 3, Nov. 2002, pp. 1858 – 1862.

[6] R. T. Burton, K. K. Isaac, J. S. Fleming, and T. B. Martonen, "Computer Reconstruction of a Human Lung Boundary Model from Magnectic Resonance Images," *Respiratory Care*, vol. 49, pp. 180 – 185, Feb. 2004.

[7] M. Betke, H. Hong, and J. P. Ko, "Automatic 3D Registration of Lung Surfaces in Computed Tomography Scans," *Medical Image Computing and Computer-Assisted Intervention - MICCAI 2001*, vol. 2208, pp. 725-733, Oct. 2001.

[8] D. Bartz, D. Mayer, S. Fischer, J. Ley, A. D. Rio, S. Thust, C. P. Heussel, H. U. Kauczor, and W. Strasser, "Hybrid Segmentation and Exploration of the Human Lungs," in *IEEE Visualization*, Oct. 2003, pp. 177-184.

[9] Y. Nakada, M. Mori, K. Mori, T. Kitasaka, Y. Suenaga, H. Takabatake, and H. Natori, "Recognition of lung lobes and its application to the bronchial structure analysis," in *18th International Conference on Pattern Recognition (ICPR)*, vol. 3, Aug. 2006, pp. 288 - 291.

[10] L. Zhang, E. A. Hoffman, and J. M. Reinhardt, "Atlas-Driven Lung Lobe Segmentation in Volumetric X-ray CT Images," *IEEE Transactions on Medical Imaging*, vol. 25, pp. 1-16, Jan. 2006.

[11] M. Antonelli, B. Lazzerini, and F. Marcelloni, "Segmentation & Reconstruction of the lung volume in CT images," in *ACM Symposium on Applied Computing*, Mar. 2005, pp. 255-259.

[12] X. Zhou, T. Hayashi, T. Hara, H. Fujita, R. Yokoyama, T. Kiryu, and H. Hoshi, "Automatic segmentation and recognition of anatomical lung structures from high-resolution chest CT images," *Computerized Medical Imaging and Graphics*, vol. 30, pp. 299-313, Aug. 2006.

[13] "The Visible Human Project : Getting the data," United States National Institute of Health, National Library of Medicine 2007.

[14] C. T. Fetita, F. Preteux, C. Beigelman-Aubry, and P. Grenier, "Pulmonary Airways 3-D Reconstruction From Multislice CT and Clinical Investigation," *IEEE Transactions on Medical Imaging*, vol. 23, pp. 1353-1364, Nov. 2004.

[15] T. B. Martonen, J. D. Schroete, and J. S. Fleming, "3D In Silico Modeling of the Human Respiratory System for Inhaled Drug Delivery and Imaging Analysis," *Journal of Pharmaceutical Sciences*, vol. 96, pp. 603-617, Mar. 2007.

[16] W. D. Wever, V. Vandecayeye, S. Lanciotti, and J. A. Verschakelen, "Multidetector CT-generated virtual bronchoscopy: an illustrated review of the potential clinical indications," *European Respiratory Journal*, vol. 23, pp. 776-782, Jan. 2004.

[17] "ELCAP Public Lung Image Database," Vision & Image Analysis Group (VIA) and International Early Lung Cancer Action Program (I-ELCAP) Labs, Cornell University, 2007.

[18] "Public Lung Database To Address Drug Response," Vision & Image Analysis Group (VIA) and International Early Lung Cancer Action Program (I-ELCAP) Labs, Cornell University, 2007.

[19] "National Cancer Imaging Archive," National Cancer Institute, 2007.

[20] "Medical Image Database," MedPix, 2007

[21] K. L. Tan, T. Tanaka, H. Nakamura, and A. Ishizaka, "Automated Extraction and Diagnosis of Lung Emphysema from Lung CT Images Using Artificial Neural Network," in *SICE-ICASE International Joint Conference*, Oct. 2006, pp. 2306-2311.

[22] S. C. B. Lo, J. J. Lin, L. Y. Hsu, Y. M. F. Lure, M. T. Freedman, R. Li, and H. Zhao, "Enhancement of lung nodule detection in temporal thoracic CT," in *Proc.SPIE*, vol. 5370, May 2004, pp. 1139-1144.

[23] T. Kitasaka, K. Mori, Y. Suenaga, J.-I. Hasegawa, and J.-I. Toriwaki, "A Method for Segmenting Bronchial Trees from 3D Chest X-ray CT Images," *Medical Image Computing and Computer Assisted Intervention - MICCAI*, vol. 2878, pp. 603-610, Nov. 2003.

[24] T. Tozaki, Y. Kawata, N. Niki, and H. Ohmatsu, "Extraction and Classification of Pulmonary Organs Based on Thoracic 3D CT Images," *Denshi Joho Tsushin Gakkai Ronbunchi*, vol. J82, pp. 1327-1338, Aug. 1999.

[25] Y. Yim, H. Hong, and G. S. Yong, "Hybrid lung segmentation in chest CT images for computer-aided diagnosis," in *7th International Workshop on Enterprise networking and Computing in Healthcare Industry (HEALTHCOM)*, Jun. 2005., pp. 378 – 383.

[26] J. Warren, T. McPhail, and T. Guerrero, "Lobe Estimating Ventilation and Perfusion from 3D CT scans of the Lungs," Rice University Computer Science, 2007, pp. 1-15.

[27] S. Hu, A. Hoffman, and J. M. Reinhardt, "Automatic Lung Segmentation for Accurate Quantitation of Volumetric X-Ray CT Images," *IEEE Transactions on Medical Imaging*, vol. 20, pp. 490-498, Jun. 2001.

[28] S. Ukil and J. M. Reinhardt, "Smoothing Lung Segmentation Surfaces in 3D X-Ray CT Images using Anatomic Guidance," in *Proceedings SPIE Conference Medical Imaging*, vol. 5340, 2004, pp. 1066-1075.

[29] V. Sauret, P. M. Halson, I. W. Brown, J. S. Fleming, and A. G. Bailey, "Study of the Three-Dimensional Geometry of the Central Conducting Airways in Man Using Computed Tomography," *Journal of Anatomy*, vol. 200, pp. 123–134, Feb. 2002.

[30] A. Schmidt, S. Zidowitz, A. Kriete, T. Denhard, S. Krass, and H. O. Peitgen, "A digital reference model of the human bronchial tree," *Computerized Medical Imaging and Graphics*, vol. 28, pp. 203-211, Jun. 2004.

[31] J. M. Kuhnigk, H. K. Hahn, M. Hindennach, M. Dicken, S. Krass, and H. O. Peitgen, "Lung lobe segmentation by anatomy-guided 3D watershed transform," *SPIE (Medical Imaging)*, vol. 5032, pp. 1482-1490, 2003.

[32] R. Shojaii, J. Alirezai, and P. Babyn, "Automatic Lung Segmentation in CT images using Watershed Transform," in *Proc. ICIP*, vol. 2, Sept. 2005, pp. 1270-1273.

[33] H. Haneishi, H. Ue, N. Takita, H. Toyama, T. Miyamoto, N. Yamamoto, and Y. Mori, "Lung image segmentation and registration for quantitative image analysis," *Nuclear Science Symposium Conference Record, 2001 IEEE*, vol. 3, pp. 1390 – 1393, Nov. 2001.

[34] T. Zrimec and S. Busayarat, "3D modelling and visualization of the human lung," in *2nd International Symposium on 3D Data Processing, Visualization and Transmission (3DPVT)*, Sept. 2004, pp. 110 – 115.

[35] A. Misra, M. Rudrapatna, and A. Sowmya, "Automatic lung segmentation: a comparison of anatomical and machine learning approaches," in *Proc. of Intelligent Sensors, Sensor Networks and Information Processing*, Dec. 2004, pp. 451-456.

[36] K. Okada, M. Singh, V. Ramesh, and A. Krishnan, "Prior-Constrained Scale-Space Mean Shift," presented at Proc. British Machine Vision Conference (BMVC), Edinburgh, 2006.

[37] S.-S. Sun, H. Li, X.-R. Hou, Y. Kang, and H. Zhao, "Automatic Segmentation of Pulmonary Nodules in CT Images," in *1st International Conference on Bioinformatics and Biomedical Engineering*: IEEE, 2007, pp. 790 - 793.

[38] N. Xu, N. Ahuja, and R. Bansal, "Object segmentation using graph cuts based active contours," *Computer Vision and Image Understanding*, vol. 107, pp. 210–224, Jan, 2007.

[39] S. Chen, L. Cao, J. Liu, and X. Tang, "Automatic segmentation of lung fields from radiographic images of SARS patients a new graph cuts algorithm," presented at Proceedings of the 18th International Conference on Pattern Recognition, Washington, DC, USA, 2006.

[40] J. Y. Lai, J. L. Doong, and C. Y. Yao, "Three Dimensional CAD Model Reconstruction from Image Data Computer Tomography," *International Journal of Imaging Systems and Technology*, vol. 10, pp. 328 - 338, Jul. 1999.

[41] R. C. Gonzalez, R. E. Woods, and S. L. Eddins, *Digital Image Processing Using MATLab*. New Jersey: Prentice Hall, 2002.

[42] G. C. Stockman and L. G. Shapiro, *Computer Vision*. New Jersey: Prentice Hall, 2001.

[43] M. Kubo, N. Niki, Y. Katawa, Y. Eguchi, H. Ohmatsu, R. Kakinuma, M. Kaneko, M. Kusumoto, M. Moriyama, M. Mori, and H. Nishiyama, "Automatic Extraction of Pulmonary Fissures from MultiDetector-Row CT Images," in *International Conference on Image Processing*, vol. 3, Oct. 2001, pp. 1091-1094.

[44] C. T. Liu, P. L. Tai, Y. J. Chen, C. H. Peng, T. Lee, and J. S. Wang, "A content-based ct lung image retrieval system for assisting differential diagnosis images collection," in *Proc. ICME*, Aug. 2001, pp. 174-177.

[45] B. Li, E. G. Christensen, E. A. Hoffman, G. McLennan, and J. M. Reinhardt, "Establishing a Normative Atlas of the Human Lung: Intersubject Warping and Registration of Volumetric CT Images," *Academy Radiology*, vol. 10, pp. 255-265, Nov. 2003.

[46] T. Zrimec and S. Busayarat, "Ray-Tracing Based Registration for HRCT Images of the Lungs," in *9th International Conference Proceeding in Medical Image Computing and Computer-Assisted Intervention – MICCAI*, vol. 4191 Oct. 2006, pp. 670-677.

[47] T. Zhang, N. P. Orton, T. R. Mackie, and B. R. Paliwal, "Technical note: A novel boundary condition using contact elements for finite element based deformable image registration," *Med. Phys*, vol. 31, pp. 2412-2415, Sept. 2004.